Evaluation of turbulence models for the air flow in a planar nozzle

Evaluación de modelos de turbulencia para el flujo de aire en una tobera plana

San Luis B. Tolentino Masgo[1,*,2]

Abstract

In gas flows at supersonic speeds, shock waves, flow separation and turbulence are produced due to sudden changes in pressure. The behavior of the compressible flow can be studied by using experimental equipment or by numerical methods with codes of the computational fluid dynamics (CFD). In the present work, the air flow is simulated in a 2D computational domain with the ANSYS-Fluent code version 12.1 for the geometry of a planar nozzle, using the Reynolds averaged Navier-Stokes (RANS) equation, with the objective of evaluating five turbulence models: SST $k-\omega$, $k-e$ standard, $k-\omega$ standard, $k-kl-\omega$ of transition and RSM. Numerical results of static pressure profiles were obtained for the walls of the nozzle and of the shock wave forms in the flow field, for two conditions of pressure ratios $rp = 2.008$ and $rp = 3.413$, which were compared with the experimental data of Hunter's work. It is concluded that the numerical results obtained with the turbulence model SST $k-\omega$ of Menter (1994) are more adjusted to the experimental data of static pressure and shock wave forms.

Keywords: Air flow, turbulence models, Shock wave, Static pressure, Planar nozzle, supersonic speed.

Resumen

En los flujos de gas a velocidades supersónicas se producen ondas de choque, separación del flujo y turbulencia debido a cambios repentinos de la presión. El comportamiento del flujo compresible se puede estudiar mediante equipos experimentales o por métodos numéricos con códigos de la dinámica de fluidos computacional (DFC). En el presente trabajo, el flujo de aire se simula en un dominio computacional 2D con el código ANSYS-Fluent versión 12.1 para la geometría de una tobera plana, utilizando la ecuación de Navier-Stokes de número de Reynolds promedio (NSRP), con el objetivo de evaluar cinco modelos de turbulencia: SST $k-\omega$, $k-e$ estándar, $k-\omega$ estándar, $k-kl-\omega$ de transición y RSM. Se obtuvieron resultados numéricos de perfiles de presión estática para las paredes de la tobera y de formas de ondas de choque en el campo de flujo, para dos condiciones de relaciones de presión $rp = 2,008$ y $rp = 3,413$, los cuales fueron comparados con los datos experimentales del trabajo de Hunter. Se concluye que los resultados numéricos obtenidos con el modelo de turbulencia SST $k-\omega$ de Menter (1994) están más ajustados a los datos experimentales de presión estática y de formas de ondas de choque.

Palabras clave: flujo de aire, modelos de turbulencia, onda de choque, presión estática, tobera plana, velocidad supersónica.

[1,*]Departamento de Ingeniería Mecánica, Universidad Nacional Experimental Politécnica "Antonio José de Sucre" Vice-Rectorado Puerto Ordaz, Bolívar, Venezuela. Autor para correspondencia ✉: sanluist@gmail.com
     http://orcid.org/ 0000-0001-6320-6864
[2]Grupo de Modelamiento Matemático y Simulación Numérica, Universidad Nacional de Ingeniería, Lima, Perú.

1. Introduction

Experimental studies of the behavior of compressible flow at supersonic speeds, are carried out in nozzles with different geometries in the divergent cross section, namely circular, oval, and rectangular among others. When a sudden change in pressure occurs in the divergent section of the nozzle, a shock wave is produced which causes that properties of the fluid such as temperature, velocity, density, among others, vary as a consequence of decompression and compression of the flow. The Mach number is the dominant parameter in the analysis of this type of flow.

Schlieren technique is a manner to obtain the shape of the shock wave, the turbulences and the separation of the flow from the nozzle walls. Such technique is recurrently employed in the field of high velocity flow, and was proposed by the German physicist August Topler in 1864 [1], who was the first to visualize the shape of the wave. It uses an optical process to capture images of the variation of the density.

The images and physical parameters of the compressible flow that are obtained in the lab, are of great importance to know its nature when subject to different variations of pressure and temperature. The magnitude of the physical parameters are obtained by direct observation, and the magnitude of other thermodynamic properties are obtained using empirical equations or mathematical models.

In the literature there are works reported about the limit layer of compressible flow [2]; the limit layer with different conditions of pressure gradient [3]; normal and oblique shock waves, Prndtl-Meyer expansive waves [4, 5] and turbulence [6].

The behavior of compressible flow can be reproduced using computational fluid dynamics (CFD) codes [7, 8], which employ mathematical models of governing equations and turbulence models [9] coupled in the equation of momentum.

Among the different geometry of laboratory experimental nozzles, it has been chosen to study the compressible flow for a flat nozzle. Figure 1 shows an image of its geometry (Hunter [10]).

Based on the one-dimensional theory, the flat nozzle shown in the image has a mean angle of 11.01° in the divergent section, which is considered to be out of design with respect to its geometry. This nozzle was designed for a pressure relationship rp=8.78 at the outlet of the divergent section, for a Mach number 2.07 and a pressure of 102.387 kPa (14.85 psi) at the inlet of the convergent section, for a stagnation temperature of 294.444 °K (530 °R) in the throat, for a Reynolds number $3, 2 \times 10^6$ [10].

It can be pointed out that the mean angle of design of the divergent section for conic nozzles is typically in the range 12-18° [11], and the same principle applies for flat nozzles.
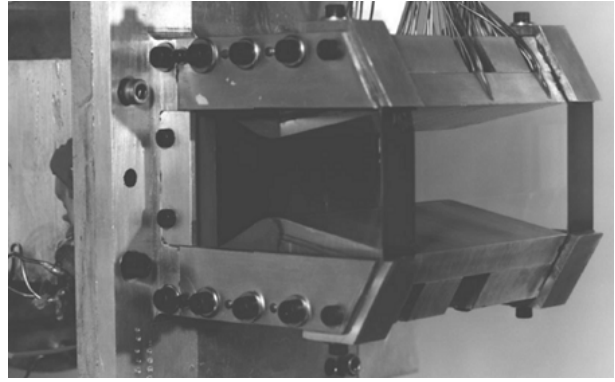

Figure 1. Photograph of a convergent-divergent flat nozzle (Hunter [10]).

Hunter [10] reported experimental results of static pressure measured at the wall of the flat nozzle, for the range of pressure relationship $rp = 1.255 - 9.543$. In addition, the flow of air was simulated for the geometry of the flat nozzle, using three turbulence models, namely Shih-Zhu-Lumley (SZL) [12], Gatski-Speziale (GS) [13] and Girimaji [14], which were compared with the experimental data of pressure for $rp = 3$, and the model SZL showed the best results.

Balabel [15] simulated the flow for the geometry of the flat nozzle [10], with the turbulence models standard $k-e$ [16], extended $k-e$ [17], v^2-f [18], realizable $v^2 - f$ [19], SST $k - \omega$ [20] and RSM [21], and compared the obtained numeric curves with experimental data of static pressure for $rp = 1.255$, $rp = 2.412$ and $rp = 5.423$. In addition, the flow was simulated using the SST turbulence model for low and high Reynolds number, also comparing with experimental data for $rp = 2.412$ and $rp = 5.423$. Based on the results, the SST $k - \omega$ turbulence model best fits the experimental data.

Besides, the geometry of the flat nozzle [10] was also used by Toufique [22], who simulated the flow with the standard $k - \omega$ turbulence model [23], and compared the shapes of the shock waves obtained with experimental data, for $rp = 2.4$ and $rp = 3.0$. Results showed that the width of the Mach disc is slightly smaller than the experimental Mach disc. Kotteda *et al.* [23] also studied the flow for different relationships of pressure and area and simulated the 2D flow with the Sparlat-Allmaras turbulence model, obtaining different configurations of the shape of the shock waves.

Other relevant works for flat nozzles with different dimensions than the flat nozzle studied by Hunter [10], are now mentioned. Forghany *et al.* [24] conducted a 2D computational research of the aerodynamic effects in the vectorization of the thrust by fluid, observing that the free flow reduces the vectorization performance and the thrust efficiency, compared to the static condition without wind.

Shimshi *et al.* [25] used experiments and 2D simulations to study the flow separation for a high Mach

number in the divergent section, and found that the transition to the asymmetric separation resulted in the jet joining the nozzle wall, and the inverse transition is accompanied by a hysteresis effect. Arora *et al.* [26] conducted experiments for the flow in a nozzle with double divergent section, observing that the angle between the two sections influences the structure of the collision.

Sivkovik *et al.* [27] conducted experiments and 2D simulations of the flow under vector control, aiming to establish a methodology of the geometry of the flow. Martelli *et al.* [28] simulated for an asymmetric 3D flow, and reported the instability of the collision and the frequency of the characteristics. Kostic *et al.* [29] simulated the 2D flow for the vector control of the thrust with different positions, obtaining the direction of the thrust force and losses.

Verma *et al.* [30] studied the unstable nature of the structure of the collision, and the results showed that the fluctuations of the pressure on the wall are accompanied of a resonance, and that the tones of such resonance ted to disappear as the pressure relationship increases and the limit layer experiments a transition.

In this work, the behavior of the flow of air in an experimental flat nozzle is simulated in a 2D computational domain [10] for five turbulence models, in order to evaluate and determine which of them produces numeric results closer to the available experimental data of static pressure and shape of the shock waves, reported in the work by Hunter [10] for $rp = 2.008$ and $rp = 3.413$.

In addition, the mathematical fundamentals, simulation results and comparison with experimental data are also presented, as well as the comparison of the numerical and experimental shapes of the shock waves. At last, the conclusions of the analysis conducted are exposed.

2. Materials and methods

2.1. Mathematical fundamentals

The four equations of fluid dynamics that govern stationary flow are the mass conservation equation

$$\nabla \cdot (\rho \vec{u}) = 0 \tag{1}$$

the energy conservation equation

$$\nabla \cdot (\rho uu) = -\nabla P + \nabla \cdot (\bar{\bar{\tau}}) \tag{2}$$

the equation of momentum

$$\nabla \cdot (\vec{u}(\rho E + P)) = \nabla \cdot (k_{eff} \nabla T + (\bar{\bar{\tau}}_{eff} \cdot \vec{u})) \tag{3}$$

and the state equation

$$\frac{\partial \rho}{\partial p} = \frac{1}{RT} \tag{4}$$

Where the tensor of tensions is expressed as $\bar{\bar{\tau}} = \mu \left[(\nabla \vec{u} + \nabla \vec{u}^T) - \frac{2}{3} \nabla \cdot \vec{u} I \right]$, with I the unit tensor, the energy is expressed as $E = h - \frac{P}{\rho} + \frac{u^2}{2}$, ρ is the density, u is the velocity, $\vec{u}$ is the velocity vector, P is the pressure, μ is the viscocity, h us the enthalpy, R is the gas constant and T is the temperature. In addition, k_{eff} is the effective conductivity, which is a function of the turbulent thermal conductivity k_t and the effective tensor of tensions $\bar{\bar{\tau}}_{eff}$.

For compressible flow, the relation of pressures and temperatures as a function of Mach number M are given by

$$\frac{P_0}{P} = \left(1 + \frac{\gamma - 1}{2} M^2 \right)^{\frac{\gamma}{\gamma - 1}} \tag{5}$$

and

$$\frac{T_0}{T} = 1 + \frac{(\gamma - 1)}{2} M^2 \tag{6}$$

respectively, where the parameters are total pressure P_0, total temperature T_0, Mach number $M = \frac{u}{c}$ and speed of sound $c = \sqrt{\gamma RT}$, where R is the gas constant and $\gamma = \frac{C_p}{C_v}$ is the relation of specific heat. Considerations on the Mach number are the following: for incompressible flow $M < 0.3$, subsonic flow $0.3 < M < 0.8$, transonic flow $0.8 < M < 1.2$, supersonic flow $1.2 < M < 3$ and hypersonic flow $M > 3$; and for flow with sonic velocity, $M = 1$ [5].

The variation of the viscosity of gases as a function of temperature can be approximated according to Sutherland law as [5].

$$\frac{\mu}{\mu_0} = \left(\frac{T}{T_0} \right)^{\frac{3}{2}} \frac{T_0 + S}{T + S} \tag{7}$$

where $\mu_0 = 1,716 \ kg/(m.s)$, is the reference viscosityia $T_0 = 273,11 \ K$, is the reference temperature and $S = 110,56 \ K$ is the effective temperature.

There are different turbulence models reported in the literature, with their respective mathematical descriptions. The turbulence models are semi-empirical transport equations that describe the mixing and diffusion that increase due to turbulent eddies, as a function of the viscosity of the fluid and the turbulent viscosity, among other variables. The models of turbulence are coupled in the linear equation of momentum, and the tensor of tensions is a function of viscosity. This mathematical expression is the Average Reynolds number Navier-Stokes equation (RANS). Besides RANS, there is the large eddies simulation model (LES) and the direct numerical simulation model (DNS). Initial research works about turbulence were conducted by Kolmogorov (1941), based on the results obtained by Reynolds (1883).

The five turbulence models used in numerical simulations by means of RANS are SST $k-\omega$ by Menter [20], standard $k-e$ by Launder and Spalding [16], standard

$k - \omega$ by Wilcox [31] and transition $k - kl - \omega$ by Walters and Cokljat [32], which are based in the turbulent viscosity and are supported by Boussinesq hypothesis. The RSM turbulence model by Launder *et al.* [21] for the pressure linear tension [33] and the effects of wall reflection [34] is supported in the tensions models by Reynolds.

2.2. Computational domain, meshing and boundary conditions

The geometry of the flat nozzle [10] studied in this work is shown in Figure 2, and the dimensions of the points of reference can be seen in Table 1.
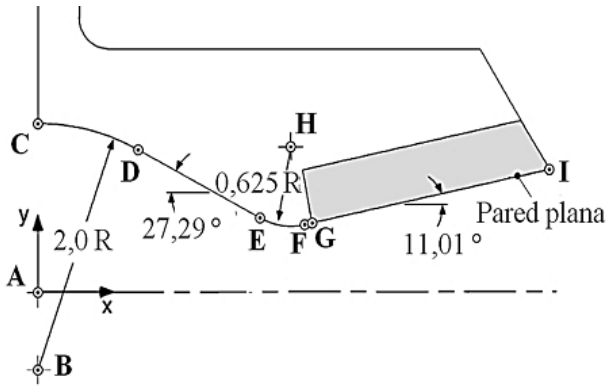

Figure 2. Schematic representation of the flat nozzle projected on the Cartesian xy plane. Adapted from Hunter [10].

Table 1. Dimensions in inches and in millimeters of the points of reference of the flat nozzle. Adapted from Hunter [10]

	Coordinate (in)		Coordinate (mm)	
Points	x	y	x	y
A	0,000	0,000	0,000	0,000
B	0,000	-0,614	0,000	-15,595
C	0,000	1,386	0,000	35,204
D	0,917	1,163	23,291	29,540
E	0,988	0,611	25,095	15,519
F	2,394	0,553	60,807	14,046
G	2,430	0,559	61,722	14,198
H	2,275	1,166	57,785	29,616
I	4,550	0,972	115,57	24,688

The geometry of the 2D computational domain can be seen in Figure 3, which is projected in the Cartesian xy plane, considering adiabatic the walls of the domain. The flow for this section was simulated due to the symmetry it possesses. The geometry of the nozzle is constructed with the dimensions in Table 1.

Before the convergent section, there is a straight segment of length $x = -25.4$ mm; the nozzle starts at $x = 0.0$ mm, the throat is located at $x = 57.785$ mm, and the divergent section of the nozzle ends at $x = 115.57$ mm; the length of the section of the atmosphere ends at $x = 471.17$ mm.
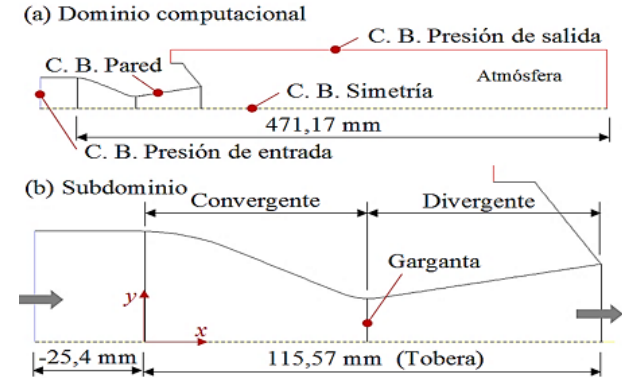

Figure 3. (a) Computational domain. (b) Subdomain: flat nozzle.

Figure 4 shows the meshed domain, which is structured in a total of 20290 quadrilateral cells. The mesh was refined towards the walls of the straight section and of the convergent-divergent section, due to the presence of shear stress in those regions.

The meshing was implemented in the ANSYS-Meshing platform, and the domain was discretized by means of the interaction ICEM-CFD. The dimensioning included: smoothing, medium; center of the expansion angle, fine; curvature of the normal angle, 18°; minimum size, 0.000249 m; maximum size of the surface, 0.0249 m; maximum size, 0.0499 m; growth relationship, 1.2; and minimum length of the boundary, 0.000914 m. For the inflation: transition relationship, 0.272; maximum layers, 2; and grow relationship, 1.2.
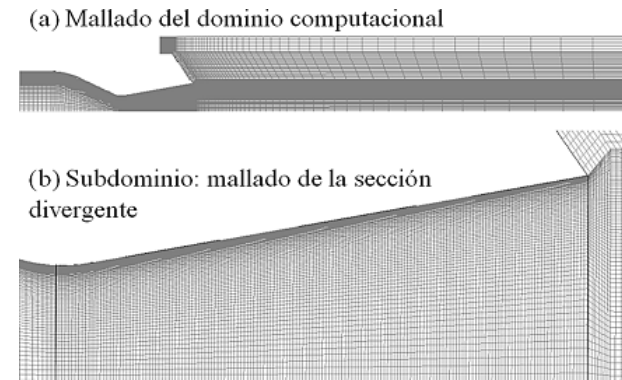

Figure 4. (a) Computational domain meshed with 20 290 quadrilateral cells. (b) Meshed of the divergent section with 11 270 quadrilateral cells.

It is important to mention that, in order to obtain a good quality of the mesh, it should be assured that each cell is not very biased, since this can generate difficulties and inaccuracies in the convergence of the numerical solutions. The most appropriate type of bias for bi-dimensional cells is the equiangular bias with Q_{EAS}, where $0 \leq Q_{EAS} \leq 1$ for any 2D cell, where

an equilateral triangle, and a square or rectangle have zero bias [35]. For the mesh with quadrilateral cells in the domain shown in Figure 4, $Q_{EAS} = 0$ for 98 % of the total cells and $Q_{EAS} = 0.3$ for the remaining 2 % of cells, resulting in a good quality mesh of the computational domain.

As part of a numerical convergence study, the mesh shown in Figure 4 yielded a satisfactory result with a final Mach number 2.0036 at the end of the divergent section in the axial symmetry, at the distance 115.57 mm for $rp = 8.78$, and using a SST $k - \omega$ turbulence model. This is an acceptable value when compared to the design value Mach 2.07 obtained by Hunter [10] at the outlet of the flat nozzle.

The initial and boundary conditions were established as:

- At the atmosphere, the outlet pressure is the total pressure $P_{atm} = 102,387 kPa$ (14,85 psi),and the total temperature $T_{atm} = 294,444K$ (530 °R).

- The total inlet pressure of the flow is established for two cases of pressure relationships $rp = 2,008$ y $rp = 3,413$ being the total input pressure $P_0 = rp \cdot P_{atm}$.

- The total inlet temperature $T_0 = 294,444K(530°R)$, is of equal magnitude than the temperature at the atmosphere. Due to the symmetry of the domain in the x axis, in the direction of the y axis the flow velocity is zero.

- The speed of the flow is zero in the adiabatic walls.

where the pressure and temperature data for $rp = 2.008$ and $rp = 3.413$, have been taken from Hunter [10].

2.3. Method of computational solution and equipment

The code ANSYS-Fluent version 12.1, which applies the finite volume method (FVM), was used for the numerical solutions of the flow of air. Among the different solution alternatives, it was chosen the option of analysis based in the density for a compressible fluid, and 2D symmetry in the Cartesian xy plane.

In each numerical simulation, a unique turbulence model was chosen in the following order: SST $k - \omega$, standard $k - e$, standard $k - \omega$, transition $k - kl\omega$ and RSM, for a total of five models. Sutherland equation was selected for the viscosity of the fluid as a function of temperature. The option Second Order Upwin was selected under the flow conditions, for the turbulence of the kinetic energy and for the type of specific dissipation. For the control solution, a Courant number equal to 2 was determined, keeping the default relaxation

factors. A fixed value of 0.00001 was determined for the residual monitor, for continuity, velocity and energy. The final results for the steady-state flow conditions were obtained after 9000-14 000 iterations.

A Síragon Laptop, model M54R, Intel Core 2 Duo, two 1.8 GHz processors and 3 GB of RAM memory, was employed for processing the data obtained in the numerical simulations.

3. Results and discussion

3.1. Comparison of the static pressure profiles with experimental data

In this section, the numerical curves of static pressure obtained for the five turbulence models, namely SST $k - \omega$, standard $k - e$, standard $k - \omega$, transition $k - kl - \omega$ and RSM, were compared with experimental data of static pressure from the work by Hunter [10], for $rp = 2.008$ and $rp = 3.413$, respectively. The profiles of static pressure correspond to the pressures along the nozzle wall, starting at the inlet of the convergent section and ending at the outlet of the divergent section.

Figure 5 shows the static pressure profiles for $rp = 2.008$, where during the drop and after a slight increase in the static pressure, the five numerical curves are close and are superimposed with the experimental data up to an estimated position $x = 70$ mm. Following these distance the numerical curves become apart with respect to each other, and then become closer in the way to the outlet of the divergent section.

In the extended detail shown in Figure 6, it can be observed how the trajectories of the numerical curves evolve after $x = 70$ mm, where the static pressure starts to increase, thus starting the separation of the flow from the wall/ The numerical curve corresponding to SST $k - \omega$ is closer to the experimental data. The RSM numerical curve exhibits an oscillatory behavior on the experimental data of pressure. The standard $k - \omega$ numerical curve has a behavior parallel to the SST $k - \omega$ curve in the upper part. At last, the numerical curves standard $k - e$ and transition $k - kl - \omega$ are very far from the experimental data in the lower part, where the minimum pressure drop occurs.

Figure 7 shows the static pressure profiles for $rp = 3.413$, which are close to the experimental data up to $x = 95$ mm, after which they become separate.

In the extended detail shown in Figure 8, it can be observed how the trajectories evolve after $x = 70$ mm. Then, after $x = 95$ mm, the standard $k - \omega$ and the SST $k - \omega$ turbulence models are superimposed, with a slight separation in the vertical direction and close to the experimental data; however, with respect to these two numerical curves, the RSM one is closer to the experimental data with small oscillations in the upper part, the standard k-e is closer in the lower part,

and the transition $k - kl - \omega$ numerical curve is the farthest from the experimental data.
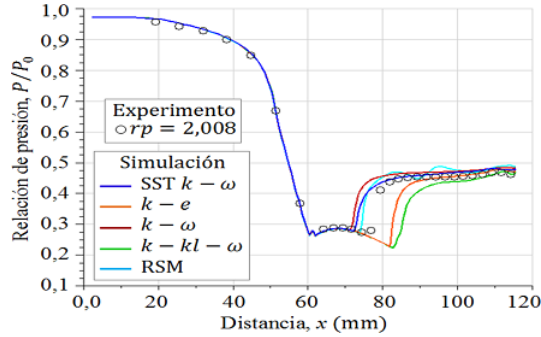

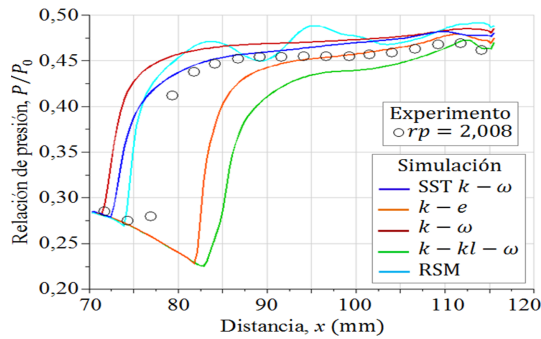**Figure 5.** Profiles of static pressure at the wall, for rp=2,008.

Figure 6. Extended detail of a section of Figure 5.
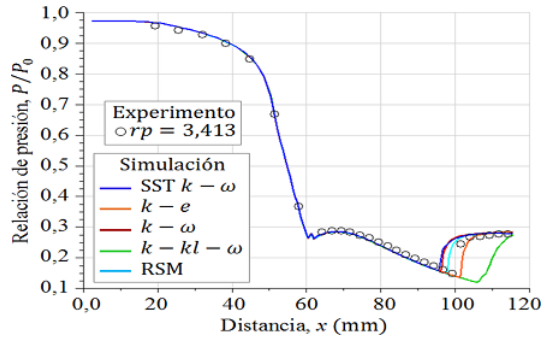

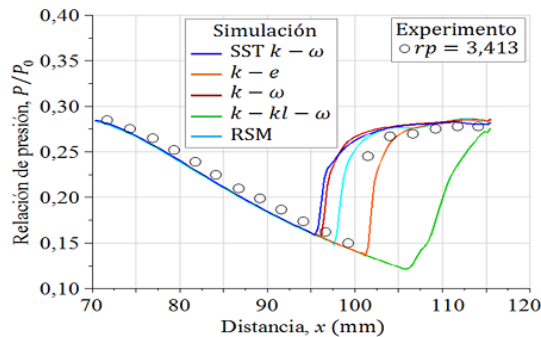**Figure 7.** Profiles of static pressure at the wall, for $rp = 3,413$.

Figure 8. Extended detail of a section of Figure 7.

From the comparison of the numerical curves in Figures 5 and 7, with respect to the experimental data of static pressure of the flat nozzle from the work by Hunter [10], the turbulence model SST $k - \omega$ by Menter [20] better approximates such experimental data.
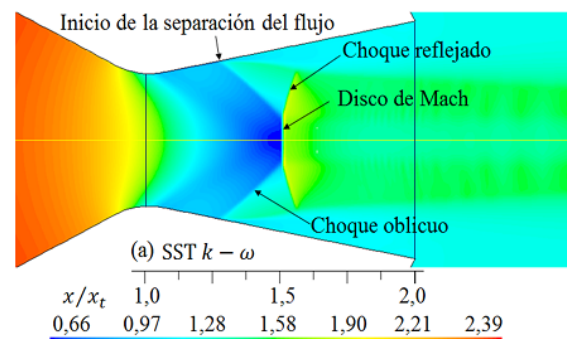
3.2. Comparison of the numerical and experimental shapes of the shock waves

The numerical simulations of the flow field with presence of shock waves in the flat nozzle, obtained for the five turbulence models are shown in Figures 9 and 10 for $rp = 2.008$, and in Figures 11 and 12 for $rp = 3.413$.

The flow of air with $rp = 2.008$ in the divergent section is over expanded, thus the shock wave is present and it can be seen which regions show the Mach disc, the oblique collision, the reflected oblique collision and the beginning of the flow separation, identifying regions in which the flow is supersonic, transonic and subsonic. The over expanded flow is characteristic when the flow decelerates in the divergent section due to an abrupt increase in the pressure, passing from a supersonic to a subsonic velocity when the collision occurs.

As the pressure of the flow increases at the inlet of the nozzle, the shock wave moves to the outlet of the nozzle. Similarly, the flow of air with $rp = 3.413$ is shown, and the over expanded flow in the divergent section also presents the Mach disc and the reflected oblique collision outside the nozzle; the divergent section is in the range of $x/x_t = 1.0 - 2.0$, where x_t is the variable distance from the position of the throat to the outlet of the nozzle, in the range 57.785-115.57 mm.

For each case, from the beginning of the flow separation downstream for the flow adjacent to the nozzle wall, a recirculation of flow is produced due to the pressure drop. As a consequence, an amount of air mass from the atmosphere is forced to enter grazing the nozzle wall.
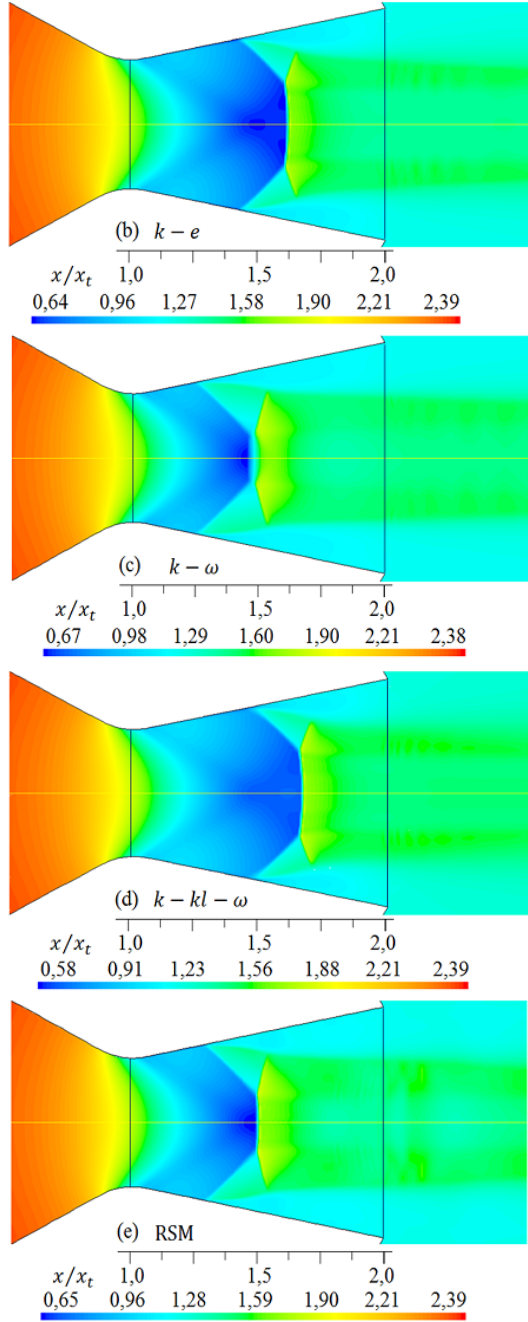
(b) $k - e$

x/x_t	1,0		1,5		2,0	
0,64	0,96	1,27	1,58	1,90	2,21	2,39

(c) $k - \omega$

x/x_t	1,0		1,5		2,0	
0,67	0,98	1,29	1,60	1,90	2,21	2,38

(d) $k - kl - \omega$

x/x_t	1,0		1,5		2,0	
0,58	0,91	1,23	1,56	1,88	2,21	2,39

(e) RSM

x/x_t	1,0		1,5		2,0	
0,65	0,96	1,28	1,59	1,90	2,21	2,39

Figure 9. Shapes of the shock waves for different turbulence models. Density (kg/m^3) of the flow for $rp = 3,413$.

(b) $k - e$

x/x_t	1,0		1,5		2,0	
0,64	0,96	1,27	1,58	1,90	2,21	2,39

(c) $k - \omega$

x/x_t	1,0		1,5		2,0	
0,67	0,98	1,29	1,60	1,90	2,21	2,38

(d) $k - kl - \omega$

x/x_t	1,0		1,5		2,0	
0,58	0,91	1,23	1,56	1,88	2,21	2,39

(e) RSM

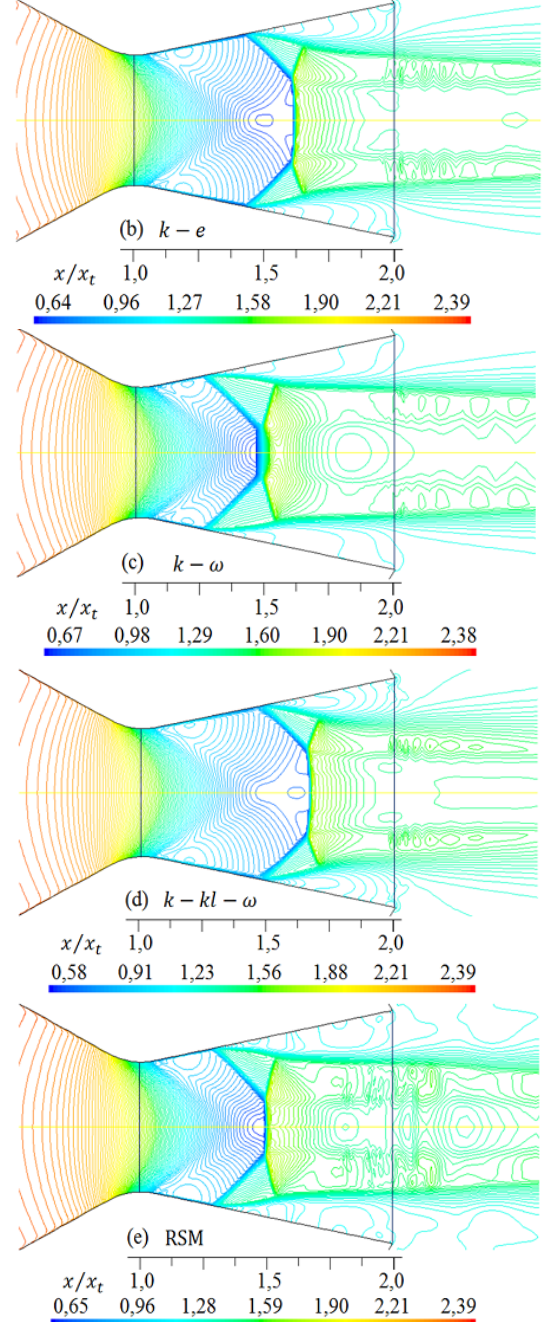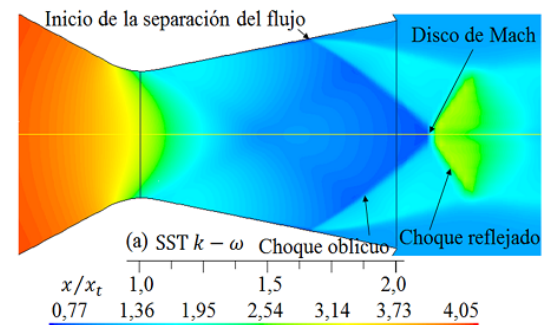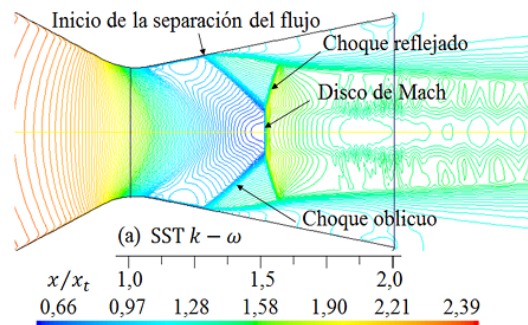| x/x_t	1,0		1,5		2,0	
0,65	0,96	1,28	1,59	1,90	2,21	2,39

Figure 10. Shapes of the shock waves for different turbulence models. Contour lines of density (kg/m^3) for $rp = 3,413$.

Inicio de la separación del flujo
Choque reflejado
Disco de Mach
Choque oblicuo
(a) SST $k - \omega$

x/x_t	1,0		1,5		2,0	
0,66	0,97	1,28	1,58	1,90	2,21	2,39

Inicio de la separación del flujo
Disco de Mach
(a) SST $k - \omega$ Choque oblicuo   Choque reflejado

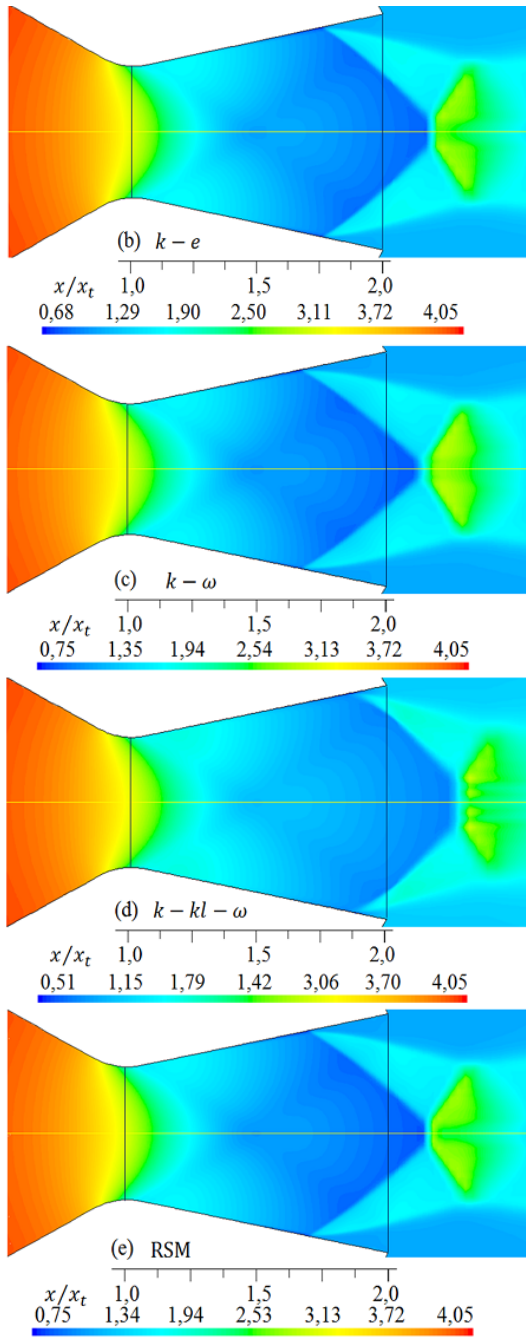| x/x_t	1,0		1,5		2,0	
0,77	1,36	1,95	2,54	3,14	3,73	4,05

Figure 11. . Shapes of the shock waves for different turbulence models. Density (kg/m^3) of the flow for $rp = 3,413$.
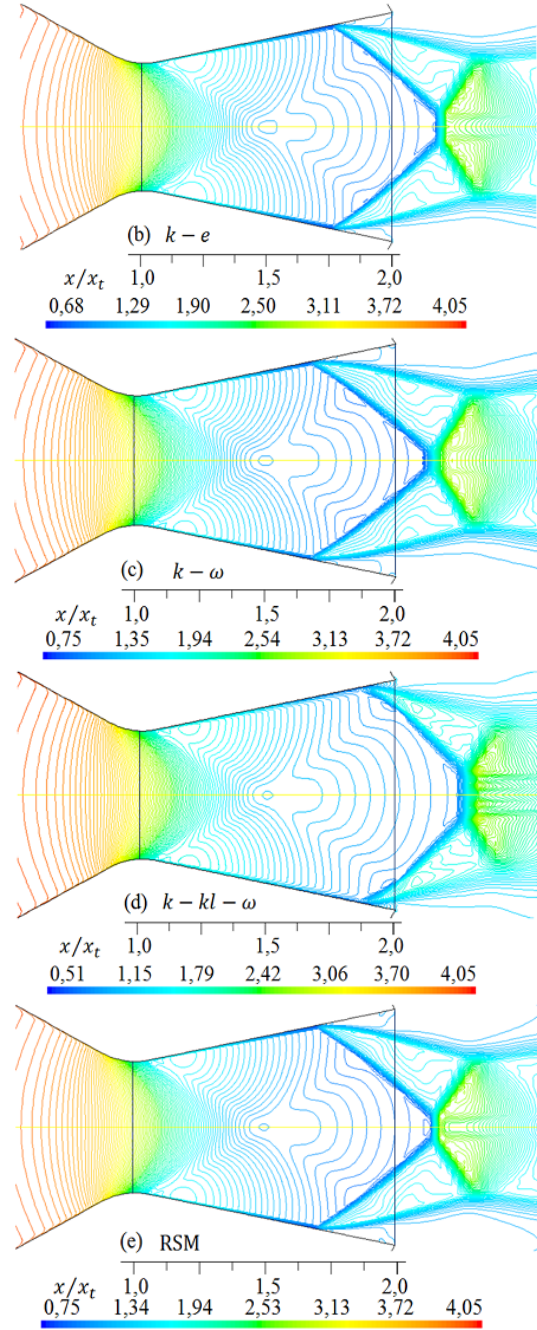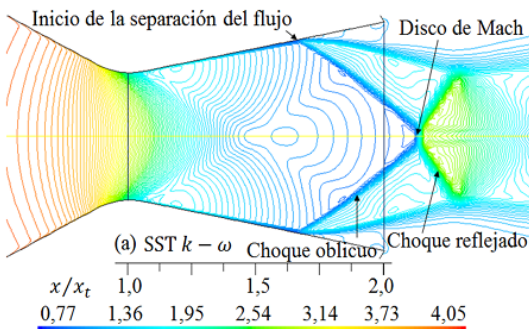

Figure 12. Shapes of the shock waves for different turbulence models. Contour lines of density (kg/m^3) for $rp = 3,413$.

The profiles of the densities of flow obtained along of the symmetry in the direction of the x axis for the five models of turbulence, are shown in Figure 13 for $rp = 2.008$, and in Figure 14 for $rp = 3.413$. For each case, it is seen the behavior of the trajectories of the numerical curves, the decrease and increase in the density where the shock wave is present.
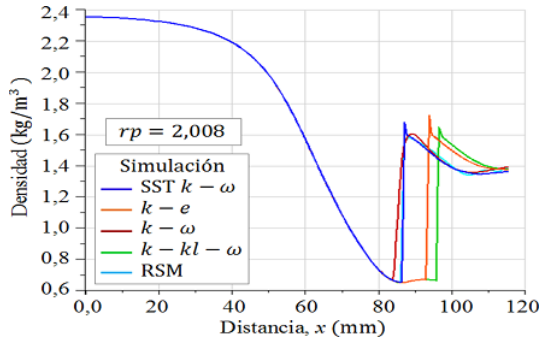
Figure 13. Density profiles evaluated at the symmetry of the x axis, for $rp = 2,008$.
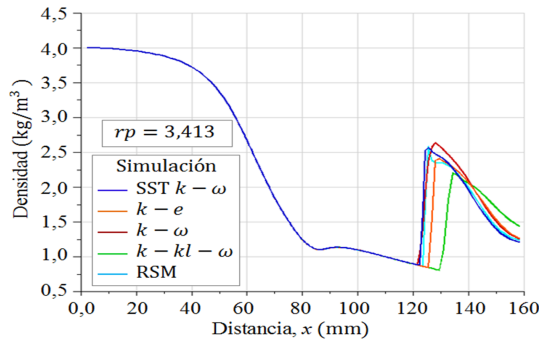

Figure 15. Shape of the shock wave for $rp = 2.008$. Adapted from the work by Hunter [10].

Figure 14. Density profiles evaluated at the symmetry of the x axis, for $rp = 3,413$.

Figure 16. Shape of the shock wave for $rp = 3.413$. Adapted from the work by Hunter [10].

After comparing the numerical results of the shapes of the shock waves in Figures 9 y 10 for $rp = 2.008$, with the shape of the experimental shock wave captured with Schlieren technique that can be observed in Figure 15 (from the work by Hunter [10]), it is seen that for the SST $k - \omega$ turbulence model, the Mach disc at the position $x/x_t = 1.5$, the oblique collision, the reflected collision and the beginning of flow separation, are similar to the experimental results. With respect to the other numerical results of the shapes of the shock waves, some are displaced to the left and some to the right, thus the Mach disc moves to the position $x/x_t = 1.5$. It can be pointed out that the Mach discs, which correspond to a normal wavefront, vary their width for each model of turbulence.

Similarly, comparing the shapes of the shock waves shown in Figures 11 and 12 for $rp = 3.413$, with the shape of the experimental shock wave in Figure 16, it can be seen that the SST $k - \omega$ turbulence model better fits the experimental result, although the Mach disc outside the nozzle is of smaller length with respect to the shape of the experimental shock wave. The other shapes of the numerical shock waves are displaced, some to the left and others to the right, thus the same will occur with the Mach disc.
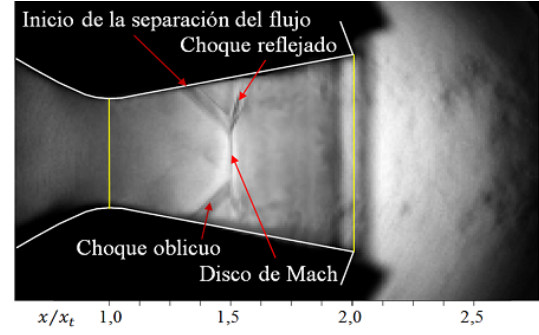
As shown in Figures 9 to 12, the shock waves vary their shape according to the turbulence model employed in the simulations, and the beginning of flow separation is not kept at a fixed position.

The experimental Mach disc for $rp = 2.008$ is at $x/x_t = 1.5$, with location $x = 86.677\ mm$, where $x_t = 57.785\ mm$. Due to difference in density, which can be appreciated by the gray scale, it can be seen that there is a thickness of the shock wave, since the flow suddenly goes from a low to a high pressure, thus the velocity of the flow suddenly decelerates in a time instant. The same occurs for the shock wave present outside of the nozzle for $rp = 3.413$ at $x/x_t = 2.11$, with location $x = 122.06\ mm$.

The numerical simulations have given for each Mach disc, the thicknesses of the wavefront in the x axis symmetry of the compressible flow domain, the position and the percentage of displacement, which are shown in Table 2 for $rp = 2.008$ and in Table 3 for $rp = 3.413$.

The simulated flow for $rp = 2.008$ shows that the position of the Mach disc coincide for SST $k - \omega$ and standard $k - \omega$, and are separated 0.0068% by the left extreme of the position of the experimental Mach disc; this displacement to the left is indicated by the negative sign in Table 2. On the other hand, by the right extreme are separated 7.86% the standard k-e, 10.96% the transition $k - kl - \omega$ and 0.61% the RSM.

The standard $k - \omega$ has the greater thickness of the Mach disc, while the transition $k - kl - \omega$ has the smallest. The Mach discs for the SST $k - \omega$, standard $k - \omega$ and RSM turbulence models have less than 1% displacement with respect to the position of the experimental Mach disc, which is acceptable in engineering; nevertheless, according to the numerical results, the SST $k - \omega$ is the turbulence model that better fits the experiment.

It should be pointed that the thickness of the Mach disc was obtained from the density profiles, in the x axis symmetry, from the initial position where the density of the flow starts to increase to the final position where the maximum compression is reached. Figure 13 shows the density increase, for the estimated range 85-90 mm, which is the region where the collision front is present for the numerical simulations.

For $rp = 3,413$, the positions of all Mach discs are displaced to the right with respect to the experimental Mach disc, as shown in Table 3. The With 1.27%, the SST $k - \omega$ has the smallest percentage of displacement, while the transition $k - kl - \omega$ has the largest percentage of displacement with 8.14%. For this case, the thicknesses of all Mach discs are greater with respect to the simulated flow for $rp = 2.008$. Similar to the previous case, the result of the SST $k - \omega$ turbulence model exhibits the best fit to the experiment.

Table 2. Thickness, position and percentage of displacement of each Mach disc with respect to the experimental Mach disc at $x = 86.677\ mm$, for $rp = 2.008$

Turbulence model	Espesor (mm)	Position x (mm)	Percentage of displacement
SST $k - \omega$	1,017	86,671	-0,007
$k - e$	1,017	93,492	7,862
$k - \omega$	5,384	86,671	-0,006
$k - kl - \omega$	0,718	96,184	10,968
RSM	2,153	87,21	0,614

Table 3. Thickness, position and percentage of displacement of each Mach disc with respect to the experimental Mach disc at $x = 122.06\ mm$, for $rp = 3.413$

Turbulence model	Espesor (mm)	Position x (mm)	Percentage of displacement
SST $k - \omega$	3,983	123,619	1,277
$k - e$	3,915	127,568	4,512
$k - \omega$	6,49	124,873	2,034
$k - kl - \omega$	4,941	131,996	8,14
RSM	3,1	124,061	1,639

For both cases $rp = 2.008$ and $rp = 3.413$, in which the flow is over expanded in the divergent section of the flat nozzle, the shapes of the shock waves obtained for the SST $k - \omega$ turbulence model have the best fit

to the experimental shock waves shown in Figures 15 and 16.

It should be pointed that a case study for the same geometry of the flat nozzle [10] considered in the present work, but with a porous surface in the flat wall of the divergent section, was conducted by Abdol-Hamid *et al.* [36], who simulated the 3D flow for the three turbulence models standard $k - e$ [16], SZL [12] and RSM [21], comparing with experimental results. The 3D results obtained in the symmetry of the flat wall, did not significantly contribute in an improvement when compared to the 2D results, for the range $1.41 < rp < 2.1$ in the pressure relationship.

For flow in domains that have symmetry, the favorable option is to simulate in 2D due to the save in hours of computational cost, which reduces the time of iteration and yields favorable results in specific regions, without having to use 3D flow simulation to obtain similar results in symmetry. Nevertheless, the 3D simulation provides relevant information away from the symmetry, in the corners of the walls, where the flow regime suddenly changes; for this it should be considered the use of turbulence models which have been already validated, and furthermore, if more precision is required in the numerical results the models LES or DNS should be employed.

The obtained numerical results are related to the mathematical fundamentals of each turbulence model, and the evaluation method applied in the region of the turbulent limit layer, because of the presence of shear stress in that region of flow. Besides, in the limit layer there are two parameters involved, namely the thickness and the friction coefficient, for both laminar and turbulent flow.

The SST $k - \omega$ turbulence model is a model of the Shear Stress Transport (SST) which employs two equations, one for the turbulent kinetic energy k, and the other for the specific dissipation rate ω, where the latter determines the turbulence scale. The mathematical expressions which are part of this structure are: the eddy viscosity, which transports the momentum by means of the turbulent eddies; the generation of turbulent kinetic energy due to gradients of mean velocity and the transverse diffusion, among other variables and constants which are used as parameters for the development of the flow regime.

This model has the ability of forecasting the behavior of the compressible fluid with more precision for opposite pressure gradients, which in the simulations demonstrates where the front of the shock wave is present in the symmetry in the direction of the x axis. The sensitivity to abrupt pressure variations, which produce the separation of flow from the divergent wall, is slightly smaller with respect to the turbulence models $k - e$ and RSM, which are closer to the experimental data.

Nevertheless, the SST $k - \omega$ turbulence model ex-

hibits better numerical results compared to the other turbulence models employed.

4. Conclusions

After evaluating the five turbulence models, namely SST $k - \omega$, standard $k - \omega$, standard k-e, transition $k - kl - \omega$ and RSM, which were employed in numerical simulations of an over expanded flow, it can be concluded that:

Regarding the profiles of static pressure obtained in the simulations along the walls of the flat nozzle, the turbulence model SST $k - \omega$ exhibited the best fit to the experimental data for the pressure relationships $rp = 2.008$ and $rp = 3.413$.

The profiles of density evaluated in the symmetry of the x axis, for $rp = 2.008$ and $rp = 3.413$, exhibit an abrupt increase in magnitude where the shock wave is present, and the SST $k - \omega$ turbulence model has the steepest slope.

The shapes of the shock waves for the field of density, obtained in the simulations with the SST $k - \omega$ turbulence model for the pressure relationships $rp = 2.008$ and $rp = 3.413$, are similar to the shapes of the experimental shock waves captured with the Schlieren technique, where for $rp = 2.008$ the Mach disc is displaced 0.007% to the left, and for $rp = 3.413$ the Mach disc is displaced 1.277% to the right.

For further works it is recommended to simulate the 3D flow and compare with the results of this work, to determine the numerical deviations that could occur with respect to the experimental data of pressure. Besides, simulate the flow with the SST $k - \omega$ turbulence model for the fields of static temperature, Mach number and pressure, to obtain the magnitude of the physical parameters before and after the shock wave.

Acknowledgement

References

[1] P. Krehl and S. Engemann, "August toepler — the first who visualized shock waves," *Shock Waves*, vol. 5, no. 1, pp. 1–18, Jun 1995. [Online]. Available: https://doi.org/10.1007/BF02425031

[2] F. White, *Viscous fluid flow.* McGraw-Hill, 1991. [Online]. Available: http://bit.ly/2Wl4Htw

[3] H. Schlichting, *Boundary-layer theory.* McGraw-Hill classic textbook reissue series, 2016. [Online]. Available: http://bit.ly/2wh45Xk

[4] J. D. Anderson, *Fundamentals of aerodynamics.* McGraw-Hill series in aeronautical and aerospace engineering, 2001. [Online]. Available: http://bit.ly/2YHGyeb

[5] F. White, *Mecánica de Fluidos.* McGraw-Hill Interamericana de España S.L., 2008. [Online]. Available: http://bit.ly/2W4dHEd

[6] T. V. Karman, "The fundamentals of the statistical theory of turbulence," *Journal of the Aeronautical Sciences*, vol. 4, no. 4, pp. 131–138, 1937. [Online]. Available: https://doi.org/10.2514/8.350

[7] J. Blazek, *Computational fluid dynamics: principles and applications.* Butterworth-Heinemann, 2015. [Online]. Available: http://bit.ly/2HRC7GM

[8] B. Andersson, R. Andersson, L. Håkansson, M. Mortensen, R. Sudiyo, B. van Wachem, and L. Hellström, *Computational Fluid Dynamics Engineers.* Cambridge University Press, 2012. [Online]. Available: http://bit.ly/2YLOcUR

[9] D. C. Wilcox, *Turbulence modeling for CFD.* DCW Industries, 2006. [Online]. Available: http://bit.ly/2K0NH5o

[10] C. Hunter, "Experimental, theoretical, and computational investigation of separated nozzle flows," *American Institute of Aeronautics and Astronautics*, 1998. [Online]. Available: https://doi.org/10.2514/6.1998-3107

[11] G. P. Sutton and O. Biblarz, *Rocket propulsion elements.* John Wiley & Sons, 2001. [Online]. Available: http://bit.ly/2WkBGxT

[12] T.-H. Shih, J. Zhu, and J. L. Lumley, "A new reynolds stress algebraic equation model," *Computer Methods in Applied Mechanics and Engineering*, vol. 125, no. 1, pp. 287–302, 1995. [Online]. Available: https://doi.org/10.1016/0045-7825(95)00796-4

[13] T. B. Gatski and C. G. Speziale, "On explicit algebraic stress models for complex turbulent flows," *Journal of Fluid Mechanics*, vol. 254, pp. 59–78, 1993. [Online]. Available: https://doi.org/10.1017/S0022112093002034

[14] S. S. Girimaji, "Fully explicit and self-consistent algebraic reynolds stress model," *Theoretical and Computational Fluid Dynamics*, vol. 8, no. 6, pp. 387–402, Nov 1996. [Online]. Available: https://doi.org/10.1007/BF00455991

[15] A. Balabel, A. Hegab, M. Nasr, and S. M. El-Behery, "Assessment of turbulence modeling for gas flow in two-dimensional convergent–divergent rocket nozzle," *Applied Mathematical Modelling*, vol. 35, no. 7, pp. 3408–3422, 2011. [Online]. Available: https://doi.org/10.1016/j.apm.2011.01.013

[16] B. E. Launder and D. B. Spalding, *Lectures in mathematical models of turbulence.* Academic Press, London, New York, 1972. [Online]. Available: http://bit.ly/2Jz9rWt

[17] Y. S. Chen and S. Kim, "Computation of turbulent flows using extended k-ε turbulence closure model," NASA Contractor report. NASA CR-179204, Tech. Rep., 1987. [Online]. Available: http://bit.ly/2HNf6VA

[18] F.-S. Lien and G. Kalitzin, "Computations of transonic flow with the $v^2 - f$ turbulence model," *International Journal of Heat and Fluid Flow*, vol. 22, no. 1, pp. 53–61, 2001. [Online]. Available: https://doi.org/10.1016/S0142-727X(00)00073-4

[19] P. Durbin, "On the $k - \varepsilon$ stagnation point anomaly," *International Journal of Heat and Fluid Flow*, vol. 17, no. 1, pp. 89–90, 1996. [Online]. Available: http://bit.ly/2EsZSnV

[20] F. R. Menter, "Two equation eddy-viscosity turbulence models for engineering applications," *AIAA Journal*, vol. 32, no. 8, pp. 1598–1605, 1994. [Online]. Available: https://doi.org/10.2514/3.12149

[21] B. E. Launder, G. J. Reece, and W. Rodi, "Progress in the development of a reynolds-stress turbulence closure," *Journal of Fluid Mechanics*, vol. 68, no. 3, pp. 537–566, 1975. [Online]. Available: https://doi.org/10.1017/S0022112075001814

[22] A. Toufique Hasan, "Characteristics of over-expanded nozzle flows in imposed oscillating condition," *International Journal of Heat and Fluid Flow*, vol. 46, pp. 70*–83, 2014. [Online]. Available: https://doi.org/10.1016/j.ijheatfluidflow.2014.01.001

[23] V. M. K. Kotteda and S. Mittal, "Flow in a planar convergent–divergent nozzle," *Shock Waves*, vol. 27, no. 3, pp. 441–455, May 2017. [Online]. Available: https://doi.org/10.1007/s00193-016-0694-4

[24] M. Taeibi-Rahni, F. Forghany, and A. Asadollahi-Ghoheih, "Numerical study of the aerodynamic effects on fluidic thrust vectoring," in *Conference: International Congress Propulsion Engineering, At Kharkov, Ukrain*, no. 8, 2015, pp. 27–34. [Online]. Available: http://bit.ly/2W1p6Ew

[25] E. Shimshi, G. Ben-Dor, A. Levy, and A. Krothapalli, "Asymmetric and unsteady flow separation in high mach number planar nozzle," *International Journal of Aeronautical Science & Aerospace Research (IJASAR)*, vol. 2, no. 6, pp. 65–80, 2015. [Online]. Available: https://doi.org/10.19070/2470-4415-150008

[26] R. Arora and A. Vaidyanathan, "Experimental investigation of flow through planar double divergent nozzles," *Acta Astronautica*, vol. 112, pp. 200 – 216, 2015. [Online]. Available: https://doi.org/10.1016/j.actaastro.2015.03.020

[27] S. Zivkovic, M. Milinovic, N. Gligorijevic, and M. Pavic, "Experimental research and numerical simulations of thrust vector control nozzle flow," *The Aeronautical Journal*, vol. 120, no. 1229, pp. 1153–1174, 2016. [Online]. Available: https://doi.org/10.1017/aer.2016.48

[28] E. Martelli, P. P. Ciottoli, M. Bernardini, F. Nasuti, and M. Valorani, "Delayed detached eddy simulation of separated flows in a planar nozzle," in *7th European Conference for Aeronautics and aerospace Sciences*, 2017. [Online]. Available: https://doi.org/10.13009/EUCASS2017-582

[29] O. Kostic, Z. Stefanovic, and I. Kostic, "Comparative cfd analyses of a 2d supersonic nozzle flow with jet tab and jet vane," *Tehnicki vjesnik*, vol. 24, no. 5, pp. 1335–1344, 2017. [Online]. Available: https://doi.org/10.17559/TV-20160208145336

[30] S. Verma, M. Chidambaranathan, and A. Hadjadj, "Analysis of shock unsteadiness in a supersonic over-expanded planar nozzle," *European Journal of Mechanics - B/Fluids*, vol. 68, pp. 55–65, 2018. [Online]. Available: https://doi.org/10.1016/j.euromechflu.2017.11.005

[31] D. C. Wilcox, "Reassessment of the scale-determining equation for advanced turbulence models," *AIAA Journal*, vol. 26, no. 11, pp. 1299–1310, 1988. [Online]. Available: https://doi.org/10.2514/3.10041

[32] K. Walters and D. Cokljat, "A three-equation eddy-viscosity model for reynolds-averaged navier-stokes simulations of transitional flows," *Journal of Fluids Engineering*, vol. 130, no. 12, p. 121401, 2008. [Online]. Available: https://doi.org/10.1115/1.2979230

[33] M. M. Gibson and B. E. Launder, "Ground effects on pressure fluctuations in the atmospheric boundary layer," *Journal of Fluid Mechanics*, vol. 86, no. 3, pp. 491–511, 1978. [Online]. Available: https://doi.org/10.1017/S0022112078001251

[34] B. E. Launder, "Second-moment closure and its use in modeling turbulent industrial flows," *International Journal for Numerical Methods in Engineering*, vol. 9, pp. 963–985, 1989. [Online]. Available: https://doi.org/10.1002/fld.1650090806

[35] Y. A. Cengel and J. M. Cimbala, *Mecánica de fluidos, fundamentos y aplicaciones.* McGraw-Hill, 2006. [Online]. Available: http://bit.ly/2X7THwU

[36] K. S. Abdol-Hamid, A. Elmiligui, C. A. Hunter, and S. J. Massey, "Three-dimensional computational model for flow in an over expanded nozzle with porous surfaces," in *Eighth International Congress of Fluid Dynamics & Propulsion, Cairo, Egypt*, 2006. [Online]. Available: https://go.nasa.gov/2JY3QZe